DC-Electrical Resistivity Imaging for embankment dike investigation: A 3D extended normalisation approach

Yannick Fargier, Sergio Palma-Lopes, Cyrille Fauchard, Daniel Francois, Philippe Cote

DC-Electrical Resistivity Imaging for embankment dike investigation: A $3D$ extended normalisation approach

Yannick Fargier[a,b,c,1,*], Sérgio Palma Lopes[b], Cyrille Fauchard[a], Daniel François[c], Philippe Côte[b]

[a] *Centre d'Études Techniques de l'Équipement - Normandie Centre, 11, rue Laplace, CS 2912, 41029 Blois Cedex, France*
[b] *LUNAM, Ifsttar, Route de Bouaye, 44230 Bouguenais, France*
[c] *EDF R&D, 6 Quai Watier, 78000 Chatou, France*

Abstract

Levee, dike and earth embankment dam structures are difficult to assess because of their length and complexity. Managers often include geophysical investigations in the overall dike condition assessment and the DC-Electrical Resistivity Imaging (ERI) method is particularly applicable owing to its cost-effectiveness and its potential sensitivity to internal erosion. However, due to the truly $3D$ nature of embankment dikes, implementing inline longitudinal tomographies along with conventional $2D$ inversion is likely to yield image artifacts. $3D$ effects from external causes (geometry, water reservoir) can be predicted and therefore we present a new approach based on redefining the normalisation principle to derive apparent resistivities from the measured data. The aim is to provide a set of pre-processed apparent resistivities that are not contaminated by external $3D$ effects and that yield more reliable results when processed within a $2D$ conventional inversion scheme. The presented approach is successfully applied to synthetic and real data sets, proving superior to the conventional $2D$ approach, although data acquisition

*Corresponding author
Email address: yannick.fargier@developpement-durable.gouv.fr, Tel +33254554932, Fax +33254554871 (Yannick Fargier)

approach is the same thus keeping the same cost-effectiveness.

Keywords: Embankment hydraulic structures, Electrical Resistivity Imaging, Apparent resistivity concept, Normalisation

1. Introduction

Hydraulic earthfill structures such as the embankment dams, dikes and levees are essential infrastructures. A variety of functions are performed by hydraulic embankments in interest of populations such as energy production, waterway freight transport, water retention and storage and protection against flood events (Fauchard and Mériaux, 2007; Royet, 2006). However, embankment dikes and dams are subject to several phenomena such as water infiltration and internal erosion, which may lead to mechanical weakness and even breaching (Foster et al., 2000a; Fell and Fry, 2007).

Stability assessment methodologies more often include geophysical investigations for the identification of weak segments and for the optimization of geotechnical testing (Carlsten et al., 1995; Mériaux et al., 2006). More precisely, the common geophysical practice includes high output investigation methods for fast zoning purposes, and DC-electrical resistivity imaging (ERI) for a higher resolution locating and characterizing of defaults (Fauchard and Mériaux, 2007; Royet et al., 2012). Thanks to recent improvements in data acquisition, ERI is now widely used for dike survey and monitoring (Hennig et al., 2005; Sjödahl et al., 2006, 2008; Tsourlos et al., 1999). Advantages of ERI based techniques are numerous. They are moderately fast to implement, cost-effective and highly sensitive to DC-electrical conductivity contrasts commonly found in dikes due to state and variability of encountered

materials (clay content, moisture content in vadose zone, temperature, porosity or compaction level) (Johansson and Dahlin, 1996). For cost-effectiveness reasons (dikes being long linear structures), ERI is usually applied in a conventional way, based on a line of equidistant electrodes parallel to the longitudinal direction (e.g. on the crest axis). When the layout includes two or more parallel lines, these are usually obtained or processed separately and inverted within two-dimensional ($2D$) type inversion schemes (except in few cases e.g.(Cho and Yeom, 2007), but still with a $2D$ type of inversion).

However, dike geometry and internal property distribution clearly violates such a simple $2D$ assumption leading to potential artifacts in resulting $2D$ images (Hennig et al., 2005; Tsourlos et al., 1999). The development of data processing techniques for improving ERI relevance for dike investigation is clearly essential. Although fully $3D$ approaches would address the problem in a more rigorous manner, they do not benefit from the cost-effectiveness of $2D$ data acquisition procedures for dike assessment.

In this context, we propose to still carry out a classical $2D$ ERI acquisition technique and then to insert external $3D$ information in the data before performing the conventional $2D$ data inversion, similarly to previously published work for other applications (Fox et al., 1980; Vickery and Hobbs, 2002). This information is included through a new data normalisation scheme that leads to apparent resistivities corrected for external $3D$ effects. In this paper, the common $2D$ ERI practice and related potential pitfalls are presented. Then, the conventional normalisation technique is i) redefined and ii) developed to address the specific limitations of dike longitudinal survey. The new normalisation approach takes into account the known neighbouring media (external

causes of $3D$ effects). Finally, this new development is applied to both synthetic and real case data sets and results are compared with conventional $2D$ inversion results.

2. Application of $2D$ ERI investigation to embankment dikes: background and limitations

2.1. Common methodology

DC-ERI method is usually used to image rapidly and efficiently variations along the longitudinal or transverse directions of the surveyed dike (Sjödahl et al., 2006, 2008). A $2D$ longitudinal survey implies the positioning of a line of electrodes along the structure whether it is on the crest, the slopes or at the toe of the dike (Figure 1(a)). But, in this case, the $2D$ assumption implies that the resistivity does not vary in the transverse direction perpendicular to the electrode line. From this point of view, a simple scheme representing a cross section of a hydraulic structure (Figure 1(b)) clearly shows that $2D$ inversion schemes cannot be used theoretically to process geo-electrical data from a longitudinal ERI survey. Obviously, the stronger the $3D$ in-situ features, the less rigourous the use of $2D$ inversion. Thus, it is important in a first approach to identify and quantify the effects related to the $3D$ behaviour of the surveyed structure and surroundings.

2.2. Potential pitfalls

Dikes and earth embankment dams are structures of which the $3D$ geometry and resistivity distribution have a disturbing effect on $2D$ inversion results. However, it is important to determine what $3D$ effects can be considered as disturbing or not. This study leads us to separate media having

an effect on the measurements in two categories: i) the media that we need to be assessed (usually the dike body and foundation) ii) neighbouring media that are not to be assessed (e.g. the water reservoir).

Consequently, the effects of the dike topography and water reservoir can be considered as disturbing. The dike topography, the geometry of the reservoir and its resistivity distribution are all information that can be measured directly. Some national regulations regarding the safety of hydraulic structures require a monitoring of the topography of the structure and the water level in the reservoir (ex: by LiDAR techniques (Mallet and Bretar, 2009)). This information can be directly supplied by the asset manager. Moreover, the electrical resistivity distribution in the water reservoir can also be measured with adequate equipment during the geophysical campaign without adding a significant cost.

We performed a parametric study to quantify the effects on the measurements caused by the dike geometry and the water reservoir. A Finite Element Method (Comsol Multiphysics software (COMSOL Multiphysics, 2009)) was used to solve the forward problem and simulate geo-electrical survey data. Main principle and results are shown Figures 2 and 3. The principle of this study was to simulate 4-electrodes (quadrupole) Wenner measurements on a dike surface, as shown in the Figure 2(a), in varying the inter-electrode spacing a and the distance d between the quadrupole and the water reservoir. The resistivity of the dike is 1000 Ohm-m whereas water resistivity is 100 Ohm-m. Then, the simulated transfer resistance (R_t) is obtained by numerically computing the potential difference between two potential electrodes divided by the injected current intensity (I). Then, the simulated R_t

is multiplied by the Geometrical Factor (GF) computed analytically (Wenner protocol for a flat homogenous half space) to obtain the apparent resistivity (ρ_a). The result of this numerical modelling is illustrated in the form of a matrix (Figure 2(b)). For this particular case (geometry, resistivity contrast), the effects of the water volume and the topography are clearly visible because the simulated apparent resistivities do not equal the resistivity of the dike body (1000 Ohm-m). A maximum negative effect (about -35 % relative to the dike resistivity) is found for an inter-electrode spacing of about 20 m and when the distance between the quadrupole and the reservoir is the lowest. Two maximum positive effects (about +20 % relative to the dike resistivity) are observed for a minimum inter electrode spacing (a=1 m) and for measurements performed on topography edges. It can be noted that when the inter-electrode spacing is greater than 40 m the apparent resistivities increase again due to the limited width of the water reservoir in the model. It is confirmed that topography artificially increases conventionnaly calculated apparent resistivities (near the convex areas) whereas it can be seen that the water has an opposite effect. However, such results cannot cover all situations and serve as master curves on the field although they give useful and qualitative information and show that 3D effects are significant.

2.3. Principle, contribution and limitation of the normalisation technique

According to Kunetz (1966) the normalisation is an operation transforming the measure of R_t into an observable that does not depend on the position of the electrodes and on the geometry of the investigated medium. This method is widely used to compare measurements and qualitatively detect anomalies (Loke, 2011). This operation is performed by means of the

following expression:

$$\rho_a = R_t^{meas} \times GF = R_t^{meas} \times \frac{\rho_h}{R_t^{mod_{\rho_h}}} \quad (1)$$

Where ρ_a represents the generalized apparent resistivity, R_t^{meas} the measured transfer resistance, GF the generalized Geometrical Factor and $R_t^{mod_{\rho_h}}$ the simulated transfer resistance on a homogeneous medium of resistivity ρ_h (the electrode positions and the medium geometry being identical in both real and synthetic models).

In consequence, Equation 1 defines the apparent resistivity as the resistivity that would be observed after the inversion of one measure alone, and assuming that the auscultated medium is homogeneous.

This principle is applied to the previous parametric study to normalize the effect of the topography. This implies to set all resistivities of the model to 1 Ohm-m by considering the reservoir and the dike as part of this homogeneous block (Marescot et al., 2006) and then apply Equation 1. Figure 3(a) presents the result of normalising the topography effect. According to this new graph Figure 3(a)(as compared to Figure 2(b)), the procedure nearly completely cancels the effect of the topography.

Indeed, apparent resistivities do not show a dependency on the geometry as they do not exceed the true dike resistivity anymore and no effects are observed near edges (convex or concave areas). The apparent resistivity decrease zone in the graph only relates to the presence of the water reservoir. Consequently, this normalisation reveals the effect of the water reservoir alone on the measurements (conductive zone, figure 3(a)). To reveal the topography effect alone, the relative variations $((\rho_{a_1} - \rho_{a_2})/\rho_{a_2})$ between the

plots Figure 2 and 3(a) are presented Figure 3(b). This result shows again that the maximum (positive and negative) topography effects stand near the changes in slope (geometry edges).

We perform complementary numerical to study the effect on the measurement of the resistivity contrast between the water reservoir and the dike body and foundation. Figure 4 shows the effects of varying the resistivity contrast between the dike body and the water reservoir on simulated measurements respectively located at (a) 4 m (b) 12 m (c) 20 m from the reservoir. According to this result, the knowledge of the resistivity contrast between the reservoir and the dike body plays a key role on the measurements.

In summary, this study shows that three parameters have significant influences on DC-resistivity measurements: i) the geometry of the overall model (dike body and reservoir), ii) the location of the electrodes (which includes electrode spacing) and iii) the resistivity contrast between the water reservoir and the dike body. Depending on the apparent resistivity definition (normalisation) used, it was shown that the apparent resistivities can account for the electrode positions (analytical GF based on a flat homogeneous half space) or for the electrode positions and the medium topography (numerical GF based on a homogeneous medium of given geometry).

2.4. Normalisation of the effect of the water reservoir

Figures 2, 3 and 4 have shown that the effect of the water reservoir can be predominant. This study also shows that it is possible to compute the theoretical effect of the water reservoir on the measurement and to normalise the topography effect. The objective of this section is to present an approach that allows to additionally normalise the water reservoir effect on the

DC-resistivity measurements. The principle of this Extended Normalisation (EN) technique is summarized in the Figure 5. As opposed to the previous normalisation technique, we numerically simulate a model composed of two blocs, the dike and the water reservoir, in an attempt to delete the effect of the water volume on the measurements by a more complete normalisation. The resistivity of the dike is set to 1 Ohm-m while the resistivity of the water reservoir is set to the reciprocal value of the resistivity ratio between the dike and the water reservoir. Similarly to the previous techniques, the new GF are simply the reciprocal of the simulated transfer resistances.

This normalisation assumes that i) the dike body and foundation bloc is homogeneous, ii) the resistivity contrast between the disturbing medium (the water reservoir) and the investigated medium (the dike) is known and iii) the geometries of both media are known.

However, even if it exists theoretical limitations, we admit here that the inversion of (even approximately) normalised apparent resistivities always leads to more reliable results than the inversion of raw data not accounting for geometry and water volume effects.

2.5. Impact of 3D effects and normalisation on inversion results

We think that is interesting to study the impact of the $3D$ effects on the imaging result. For this purpose, we present a numerical test of the gradually more complete normalisations (1: with a conventional GF, 2: with a generalized GF, 3: with the EN technique). The test is based on a model presenting a more complex geometry (varying cross-section) and six cylindrical heterogeneities crossing the dike body in the transverse direction (Figure 6). In this numerical study, a $2D$ longitudinal ERI survey was simulated

on the dike under load condition. The width of crest is 6 m. A Wenner-Schlumberger acquisition protocol was used (690 quadripole measurements) and the inter-electrode spacing is 4 m. The resistivity of the dike body was 2000 Ohm-m and its height varies from 0 to 6 m. The six transverse heterogeneities are located in the dike body at different depths. Their resistivity is set to 80 Ohm-m equal to that of the water reservoir. The transfer resistances simulated are then processed with the $2D$ inversion software Res2Dinv (Loke and Barker, 1996a) yielding 2D resistivity sections shown in the Figures 7(a) to 7(c) using the default inversion parameters. Figure 7(a) is obtained with the raw data (ρ_a) for which only the electrodes positions is accounted for and the other effects (topography and water reservoir) are not normalised. Figures 7(b) and 7(c) show respectively the inversion results after removing the effect of the dike topography and after removing the combined effects of the topography and water reservoir. This result clearly shows that the more conductive layer (Figure 7(a) and 7(b)) is in fact an artifact due to the effect of the water reservoir on the simulated measurements and that the highly resistive zone on the right hand side of the upper layer Figure 7(a) is partly influenced by the dike topography. Figure 7(c) shows that the locating of the six anomalies (due to the modeled heterogeneities) is clearly improved by applying the EN technique.

This normalisation technique supposes that a single resistivity ratio (contrast) is selected to compute all measured apparent resistivities over the whole dike surface. However, a real embankment dike is never homogeneous and its resistivity distribution remains unknown. Consequently, in real cases, the resistivity ratio between the dike and the water reservoir cannot be consid-

ered as unique for a whole set of DC-resistivity measurements. Thus, the natural variability in embankment dikes and dams restricts the applicability of the suggested "EN" technique.

In order to demonstrate this limitation an additional synthetic test was performed. This study is similar to that used in the previous test (figure 6) except that the dike body is now composed of two contrasting stretches (Figure 8(a)): A resistive stretch on the left hand side (2000 Ohm-m) and a more conductive stretch on the right hand side (1000 Ohm-m).

Figures 8(b) to 8(d) present the results at the 4^{th} iteration of the 2D-inversion process (also based on the Res2dinv software). Figure 8(b) shows the resistivity section obtained when inverting data without normalisation approach. Figure 8(c) presents the case where the resistivity ratio is selected at its maximum value (2000/80=25) and shows a resistive layer artifact on the right hand side of the model due to the over-estimation for the resistivity contrast for this area. Figure 8(d) presents the opposite case with a conductive layer artifact on the left hand side due to an under-estimated resistivity contrast (1000/80=12.5). This result clearly shows that neglecting the spatial variability of the dike body when normalising the data inevitably underestimates (or inversely, overestimates) the resistivity contrast between the water reservoir and the investigated embankment. This leads to an unsuitable normalisation level (too strong or too weak) of the $3D$ external effects which in turn causes artifacts in the resulting image.

3. An Enhanced Extended Normalisation approach

3.1. Concept

The previous section discusses two main limitations restricting the use of the EN technique : i) the resistivity contrast between the water reservoir and the dike has to be known to a certain accuracy level ii) The resistivity distribution of the dike body has to be sufficiently constant (homogeneous medium). In order to overcome these restrictions, we present a new approach that Enhances the Extended Normalisation (EEN) technique and better matches the original apparent resistivity definition (Kunetz, 1966).

As a consequence of Kunetz (1966) apparent resistivity definition (as derived in Equation 1), one can say that in the trivial case of a homogeneous medium (of arbitrary geometry) the apparent resistivity equals the true resistivity, irrespective of the medium geometry. Conversely, one can postulate that the inversion of a single measurement to adjust a single model parameter (the "true" resistivity of the investigated medium assumed to be homogeneous) would lead this true resistivity to tend to the measured apparent resistivity. Therefore, we suggest in this paper that an apparent resistivity can be considered as the result of a basic inversion process for which the particular electrode positions are considered and the model is assumed to be homogeneous. Although in real cases the medium can rarely be considered homogeneous, one can still carry out such a straightforward inversion for each individual measured apparent resistivity. This concept is the basis of the procedure presented in the following sections.

3.2. Methodology

The method presented within the framework of this article takes the form of a pre-processing function. This method modifies the measured data into apparent resistivities corrected for the effects of the topography and the water reservoir and partly accounting for the inhomogeneity of the dike body. This methodology, schematized Figure 9, introduces three kinds of input parameters:

$$\mathbf{DEM} = [\mathbf{X}_{topo}, \mathbf{Y}_{topo}, \mathbf{Z}_{topo}]; \tag{2}$$

$$\rho_{water}^{mes}; \tag{3}$$

$$\mathbf{d}^{mes} = \begin{bmatrix} \rho_{a_1}^{mes} & \rho_{a_2}^{mes} & \dots & \rho_{a_N}^{mes} \end{bmatrix}^T; \tag{4}$$

DEM is a matrix containing elevation data used for building the numerical model (dike and reservoir). ρ_{water}^{mes} is the DC-electrical resistivity of the water reservoir. $\mathbf{d}^{mes}$ represents the vector of the measured data (apparent resistivities), N is the number of quadrupole measurements. The procedure consists in two steps as follows.

3.2.1. Step 1

The objective of *Step*1 is to provide the "mean" resistivity of the dike needed as an input to *Step*2. A basic inverse problem is used for which the inverse model is only composed of two inversion "cells" (dike body and water reservoir). Within these cells of known geometry, the model is considered to be homogeneous. Therefore, only two model parameters are needed.

$$\mathbf{m}_{step1} = \begin{bmatrix} \rho_{dike} & \rho_{water} \end{bmatrix}^T; \quad (5)$$

Where ρ_{water} is the resistivity of the water reservoir medium and ρ_{dike} that of the dike body medium. In order to perform the inversion, the matrix of Fréchet derivatives is built by calculating the pole-pole sensitivities by means of the adjoint state method (Park and Van, 1991) and then by recombining the pole-pole to get the sensitivities associated to the electrode arrays (quadrupoles) in the acquisition protocol. The finite element method (see section 2.2) is used, with mesh deformation to simulate the topography, to solve the forward problem and compute the sensitivity matrix $\mathbf{G}_{step1}$:

$$\mathbf{G}_{step1} = \begin{bmatrix} \frac{\delta \rho_{a_1}^{mes}}{\delta \rho_{dike}} & \frac{\delta \rho_{a_1}^{mes}}{\delta \rho_{water}} \\ \frac{\delta \rho_{a_2}^{mes}}{\delta \rho_{dike}} & \frac{\delta \rho_{a_2}^{mes}}{\delta \rho_{water}} \\ \vdots & \vdots \\ \frac{\delta \rho_{a_N}^{mes}}{\delta \rho_{dike}} & \frac{\delta \rho_{a_N}^{mes}}{\delta \rho_{water}} \end{bmatrix}; \quad (6)$$

As shown in Equation 6, the dimension of this sensitivity matrix is only [N,2] (which is quite different from most sensitivity matrices usually appearing in discrete geophysical inversion). The "effective" mean model $\mathbf{m}_{step2}$ is then adjusted by solving the basic inverse problem as follows (7) :

$$(\mathbf{G}_{step1}^T \mathbf{W}_d^T \mathbf{W}_d \mathbf{G}_{step1} + \lambda_{step1} \mathbf{I}_{step1}) \mathbf{m}_{step2} = \mathbf{G}_{step1}^T \mathbf{W}_d^T \mathbf{W}_d (\mathbf{d}^{mes}) \quad (7)$$

where the diagonal of the matrix $\mathbf{W}_d$ contains estimated measurements uncertainties and $\mathbf{I}_{step1}$ is the [2x2] identity matrix and $\lambda_{step1} = [\lambda_{dike}, \lambda_{water}]^T$ is the damping factor which can be different for the water and the dike

terms. Depending on the reliability of the *a priori* information on the water resistivity, a more or less high damping factor is selected for adjusting the resistivity of the water part of the model. However, the inverse problem is well-determined. so, the choice of these parameters does not modify the result radically. Finally, this step supplies resistivities for both the dike body and the water reservoir considered as homogeneous and that best explains the measured data in the sense of a least squares criterion.

$$\mathbf{m}_{step2} = \left[\begin{array}{cc} \rho_{dike}^{step2}, & \rho_{water}^{step2} \end{array} \right]^T; \tag{8}$$

However, this could have been performed, more simply but less accuratly, by selecting the mean of the shallowest apparent resistivity measurements (lowest inter electrode spacing) to limit the topography and reservoir effects (Figure 4).

3.2.2. Step 2

The only objective of the previous step is to provide an initial model for the main step presented here. The role of this main step is to yield apparent resistivities corrected for the effect of the water reservoir and the topography and accounting for the medium inhomogeneities.

Following the concept introduced in section 3.1, the idea is to estimate a resistivity for the dike body seen as homogeneous that best fits each measurement considered alone. Thus, by inverting individually each measurement gets one dike resistivity per measured datum and ends up with N resistivities. As previoulsly stated, it can be inferred from the apparent resistivity definition (Kunetz, 1966) that each resistivity estimated alone should then

be regarded as an apparent resistivity that accounts for the medium geometry. In addition here, we propose that this apparent resistivity correction accounts for the presence of a water reservoir and supports dike body inhomogeneity. Therefore, we extend the concept saying that each apparent resistivity corrected for topography and water reservoir effects should be seen as a corresponding resistivity for the dike body considered as homogeneous. To achieve this step a new inverse problem is developed (Equation 9) :

$$(\mathbf{G}_{step2}^T \mathbf{W}_d^T \mathbf{W}_d \mathbf{G}_{step2} + \lambda \mathbf{I}_{step2}) \delta \mathbf{m}_{pert} = \mathbf{G}_{step2}^T \mathbf{W}_d^T \mathbf{W}_d (\mathbf{d}^{mes} - \mathbf{d}^{calc}) \quad (9)$$

Two new variables must be computed to solve this equation:

1. The modeled apparent resistivities ($\mathbf{d}^{calc}$);

$$\mathbf{d}^{calc} = \begin{bmatrix} \rho_{a_1}^{calc} & \rho_{a_2}^{calc} & \dots & \rho_{a_N}^{calc} \end{bmatrix}^T ; \quad (10)$$

2. The matrix of the Fréchet derivatives ($\mathbf{G}_{step_2}$).

$$\mathbf{G}_{step2} = \begin{bmatrix} \frac{\delta d_1^{calc}}{\delta \rho_{dike}} & 0 & \cdots & 0 & \frac{\delta d_1^{calc}}{\delta \rho_{water}} \\ 0 & \frac{\delta d_2^{calc}}{\delta \rho_{dike}} & \cdots & 0 & \frac{\delta d_2^{calc}}{\delta \rho_{water}} \\ \vdots & \vdots & \ddots & \vdots & \vdots \\ 0 & 0 & \cdots & \frac{\delta d_N^{calc}}{\delta \rho_{dike}} & \frac{\delta d_N^{calc}}{\delta \rho_{water}} \end{bmatrix} ; \quad (11)$$

These two parameters are obtained by solving a complete forward problem with the determined resistivities of water reservoir and dike body from $Step1$. In the sensitivity matrix (Equation 11), the left-hand side $[N \times N]$ diagonal block expresses the concept of each measurement being inverted individually.

This is obviously different from usual sensitivity matrices where all data may be sensitive to all model parameters. Even though all N inversion parameters m_1 to m_N represent the same physical parameter (the resistivity of the dike body when assumed homogeneous), they have different values for each measurement and have to be considered separately. Thus, they are N distinct parameters. In cases where the water resistivity and the reservoir geometry are well known (reliable a priori information), this diagonal block can be considered alone. This leads to a trivial scheme (equivalent to N independent processes individually applied to each measured datum). In the sensitivity matrix (Equation 11), we propose to add the right-hand side column to simultaneously estimate the water resistivity.

In the framework of this study, we prefer keeping the resistivity of the water reservoir as a free parameter of which range can be controlled by adjusting a damping factor (for example : $\lambda_{reservoir} = 1000 \times \lambda_{dike}$). This leads to the more general case where the water resistivity may be known inaccurately or may slightly vary in space and time.

The solution of Equation 9 is a perturbation vector $\delta\mathbf{m}_{pert}$ that allows to update the inversion "model" containing the corrected apparent resistivities ρ_a^{corr} following Equation 12 :

$$\rho_a^{corr} = [\rho_{dike}^{step2} + \delta\mathbf{m}_{pert}(1:N), \rho_{water}^{step2} + \delta\mathbf{m}_{pert}(N+1)] \tag{12}$$

Thus, the corrected ρ_a^{corr} are the output of the presented pre-processing method, supplying the apparent resistivities that can be processed with $2D$ type of inversion software.

3.3. Synthetic results

The EEN technique is applied to the numerical study presented Figure 8 and presented in the section 2.5 (same model, same acquisition protocol) with 6 anomalies buried in a double-compartment dike. The objective is to demonstrate the added value of the new normalisation procedure. Figure 10 shows the inversion result obtained with data normalized with the new method (EEN) and using the Res2Dinv commercial software. in order to obtain the corrected apparent resistivities we impose $\lambda_{dike} = 0.01$ and $\lambda_{water} = 10$ during $Step1$ and $Step2$ and a measurement noise of 0.5%. The mean resistivities resulting from $Step1$ are 1324 ohm-m and 80.1 ohm-m for the dike and reservoir respectively.

The presented imaging result corresponds to the 4^{th} iteration with a RMS value lower than 1 %. This result shows the superiority of the new technique in this case as very few artifacts are present in the inversion result compared to Figures 8(a) to 8(c) where false layers could be denoted. Moreover, a better assessment of the anomalies is performed allowing a more robust interpretation of the imaging result.

4. Case study

A survey in high output conditions ("roll-along" longitudinal survey) was performed in situ on a dike owned and managed by EDF (Electricité De France) in the Southern France (Figure 11) in the framework of a more general assessment campaign. For this purpose, 96 electrodes were aligned with a 5 m electrode spacing on the central axis of the crest. The investigated dike is a water retaining structure leading water to a very close hydro-electricity

production plant and was in full load condition at the time of the DC-ERI survey. The dike is 6 to 7 m high. The sealing is ensured by a concrete facing on the upstream side. We measured the resistivity of water on the surface of the reservoir with various locations and found a constant value of 80.2 ohm-m $\pm$0.5 ohm-m. A Wenner-Schlumberger acquisition procedure including 1502 quadrupole measurements was performed. Figure 11 shows the electrode cable layout near the location of the water reservoir. Available information on the construction phase and the geological context of the area indicate that the dike body is composed of recent coarse alluvial deposits exploited in the vicinity and corresponding to the foundation of the structure.

Figure 12 presents the imaging results obtained with the Res2Dinv software for various normalisation levels applied to the same measured data set. Concerning the inversion parameter λ, we imposed the same parameters as for the synthetic case (ratio=1000) and an equivalent noise measurement. The mean resistivities resulting from *Step*1 are 1429 ohm-m and 79.9 ohm-m for the dike and reservoir respectively. The first global conclusion that would arise from the upper resistivity sections 12(a) with no normalisation of the reservoir or topography is that the dike is composed of two layers horizontal layers of varying thicknesses. The upper layer (5 to 8 m thick) appears to be more resistive (about 1000 to 2000 ohm-m) and shows some resistivity variations. The lower layer seems significantly less resistive (100 to 500 ohm-m) and could be interpreted as the alluvial substratum of varying upper limit (between 8 and 12 m deep below the crest). These results show that the normalisation of the topography effect alone (Figure 12(b)) lowers the overall resistivity of the dike body and leaves room for what could be seen as

an intermediate layer (upper limit between 3 and 6 m deep below the crest). The third result (Figure 12(c)) indicates that adding the normalisation of the water reservoir effect tends to push away the presumed conductive layer that could be seen at the bottom of the resistivity section (12(a) and (b)) and therefore increases the interpreted thickness of the dike body up to 13 m. Consequently, it can be concluded that this previous conductive layer in sections 12(a) and (b) is partly an artifact due to the effect of the water reservoir on the measured data. Moreover, the inversion result presented on Figure 12(c) (based on the normalisation extended to the water reservoir effect) shows some new heterogeneities between the dike body and the foundation (x=200 m) which may be critical for the safety assessment of the structure (internal erosion below the foundation). The last inversion result (Figure 12(d)) shows a very similar result to the previous one (12(c)) although it tends to limit significantly more the presence of the lower conductive layer, which will be discussed in the following section.

Concerning the four inversion results (figure 12) we do not prefer to say that a result is better than another, each one bringing of additional details. We think that the better interpretation consists in comparing the results between them in order to see the possible $3D$ pitfalls. In this manner a more robust interpretation can be performed.

4.1. Discussion

In the previous result (Figure 12(d)) presenting a 2D-inversion of real data corrected for the combined topography and water reservoir effects, the bottom conductive layer was not fully removed. Consequently, two interpretations can be proposed.

From an optimistic point of view, one can say that this layer actually exists and that the correction procedure performed well providing a reliable image of the resistivity section.

From an opposite point of view, one could conclude that the subsisting conductive layer is an artefact due to an incomplete correction of the combined topography and water reservoir effects. This incomplete normalisation can come from resistivity variations in the water reservoir not taken into account. Those variations can have an effect on the measurements, especially for high resistivity contrast between the dike body and the water reservoir. A solution would be to accuratly measure the resistivity variations in the water reservoir and to impose this distribution during the inversion process.

Finally, a more realistic point of view is to conclude that the presented correction approach has proved some efficiency although some 3D combined effects (due to the water reservoir and other external media, the topography and the internal resistivity distribution of the dike body) still remain. It can be noted that such combined 3D effects cannot be supported by a data normalisation or correction procedure and can only be delineated by means of a fully 3D acquisition and inversion process. It could be noted that the study focuse on quite homogenous structures. Structures such as earth embankment dams often have strong heterogeneities (concrete or clay core) that could reinforce this phenomenon.

Moreover, this study presents a successful outcome for the new normalisation because the dike body present a strong contrast between the dike body and the water reservoir. In less contrasting cases, one can anticipate that the added value of the EEN technique would be lower.

The EEN procedure does not add a cost to the survey except for the water resistivity measurement. Concerning the computational cost, as we can see in Figure 9, in addition to the stage of inversion, this technique requires the calculation of 1 to 2 additional 3D forward problems as well as the calculation of two matrices of Fréchet derivatives of size Nx4. In general, for a common longitudinal DC-ERI survey based on 96 inline electrodes, this correction approach needs 10 minutes for the processing of 1500 quadrupole measurements with an E5405 Intel Xeon @2 GHz CPU and requires less than 4 Gb of RAM.

5. Conclusion

Nowadays, $2D$-ERI is a commonly employed method within the overall condition assessment methodology hydraulic embankment structures. However, the use of a $2D$ inversion scheme leads to artifacts due to combined $3D$ effects. Those artifacts are often interpreted as real layers (alluvial foundation for the water reservoir effect) or anomalies and limit the robustness of the interpretation and the assessment of real anomalies. Numerical studies are used to demonstrate and quantify some 3D effects specific to dike investigations and their impact on the reconstructed models for $2D$ longitudinal surveys. Then a classical technique, the normalisation, is redefined and used to suppress the topography effects on the data. This technique is extended to the normalisation of the effect of the water reservoir in the case of dike in load condition. First, we simply assume that the embankment dike is homogeneous and second, we enhance this concept to arbitrary resistivity distributions. Results show that the EEN technique is able to support the

non-homogeneity of the dike body and to satisfactorily suppress the effect of the water reservoir. When applied to real data, this new approach leads to an improved interpretation of the survey. Consequently, the technique proves usefull when data are contaminated by "external" $3D$ effects of which causes (topography, external neighbouring media such as a water reservoir) are well documented or directly identifiable on site without adding a real cost to the survey campaign. In this context, this technique could also be employed to normalise the effect of sheet piles, concrete facing and internal networks on measurements. It can be noted, that the effect of an internal core (rockfill dams for example) on the EEN procedure has not been studied in this paper. Authors think that these hydraulic structures deserve specific attention (due to internal erosion) and further research. Our approach cannot account for all $3D$ effects, particularly those due to the actual dike resistivity distribution ("internal" causes). In conclusion, further studies are needed to build cost-effective inversion strategies well-adapted to long dike investigation at reasonable speed.

Acknowledgment

The authors wish to thank EDF-CIH as well as the research projects ERINOH and DOFEAS for the funding and access to the site, and more particularly Jean Robert Courivaud and Julien Cintract for the assistance on site. We also thank Dr Mathieu Le Feuvre and the reviewers for the discussions and their impact on the article.

References

Carlsten, S., Johansson, S., Worman, A., 1995. Radar techniques for indicating internal erosion in embankment dams. Journal of Applied Geophysics 33, 143–156.

Cho, I.K., Yeom, J.Y., 2007. Crossline resistivity tomography for the delineation of anomalous seepage pathways in an embankment dam. Geophysics 72, G31–G38.

COMSOL Multiphysics, 2009. COMSOL Multiphysics User's Guide. Version 3.5a, COMSOL AB, Stockholm, Sweden.

Fauchard, C., Mériaux, P., 2007. Geophysical and geotechnical methods for diagnosing flood protection dikes. Guide for implementation and interpretation. Editions Quae, 124 p.

Fell, R., Fry, J.J., 2007. The state of the art of assessing the likelihood of internal erosion of embankment dams, water retaining structures and their foundations. *Internal Erosion of Dams and their foundation.*

Foster, M., Fell, R., Spannagle, M., 2000a. The statistics of embankment dam failures and accidents. Canadian Geotechnical Journal 37, 1000–1024. `http://www.nrcresearchpress.com/doi/pdf/10.1139/t00-030`.

Fox, R.C., Hohmann, G.W., Killpack, T.J., Rijo, L., 1980. Topographic effects in resistivity and induced polarization surveys. Geophysics 45, 75–93.

548 Hennig, T., Weller, A., Canh, T., 2005. The effect of dike geometry on
549 different resistivity configurations. Journal of Applied Geophysics 57, 278–
550 292.

551 Johansson, S., Dahlin, T., 1996. Seepage monitoring in an earth embank-
552 ment dam by repeated resistivity measurements. European Journal of
553 Environmental and Engineering Geophysics 1, 229–247.

554 Kunetz, G., 1966. Principle of direct current resistivity prospecting. Geoex-
555 ploration monograph series 1.

556 Loke, M.H., 2011. Lectures notes on 2-D and 3-D electrical imaging surveys.
557 http://www.geotomosoft.com.

558 Loke, M.H., Barker, R.D., 1996a. Rapid least-squares inversion of appar-
559 ent resistivity pseudosections by a quasi-newton method. Geophysical
560 Prospecting 44, 131–152.

561 Mallet, C., Bretar, F., 2009. Full-waveform topographic lidar : state-of-the-
562 art. ISPRS Journal of Photogrammetry and Remote Sensing 64, 1–16.

563 Marescot, L., Rigobert, S., Palma Lopes, S., Lagabrielle, R., Chapellier,
564 D., 2006. A general approach for dc apparent resistivity evaluation on
565 arbitrarily shaped 3d structures. Journal of Applied Geophysics 60, 55–67.

566 Mériaux, P., Venntier, M., Aigouy, S., Hoonakker, M., Zylberblat, M., 2006.
567 Diagnosis and management of plant growth on embankment dams and
568 dykes, in: ICOLD, 22nd Conference on Large Dams, Barcelone, 551-567.

569 Park, S.K., Van, G.P., 1991. Inversion of pole-pole data for 3-d resistivity
570 structure beneath arrays of electrodes. Geophysics 56, 951–960.

571 Royet, P., 2006. La surveillance et l'entretien des petits barrages. Ed. Cema-
572 gref, 78 p.

573 Royet, P., Palma Lopes, S., Fauchard, C., Mériaux, P., Auriau, L., 2012.
574 Rapid and cost-effective dike condition assessment methods: geophysics
575 and remote sensing. Technical Report. Deliverable 32, FP7-ENV-2009
576 FloodProBE project.

577 Sjödahl, P., Dahlin, T., Johansson, S., Loke, M.H., 2008. Resistivity mon-
578 itoring for leakage and internal erosion detection at hällby embankment
579 dam. Journal of Applied Geophysics 65, 155–164.

580 Sjödahl, P., Dahlin, T., Zhou, B., 2006. 2.5d resistivity modeling of em-
581 bankment dams to assess influence from geometry and material properties.
582 Geophysics 71, G107–G114.

583 Tsourlos, P.I., Szymanski, J.E., Tsokas, G.N., 1999. The effect of terrain
584 topography on commonly used resistivity arrays. Geophysics 64, 1357–
585 1363.

586 Vickery, A.C., Hobbs, B.A., 2002. The effect of subsurface pipes on apparent-
587 resistivity measurements. Geophysical Prospecting 50, 1–13. Geophys.
588 Prospect.

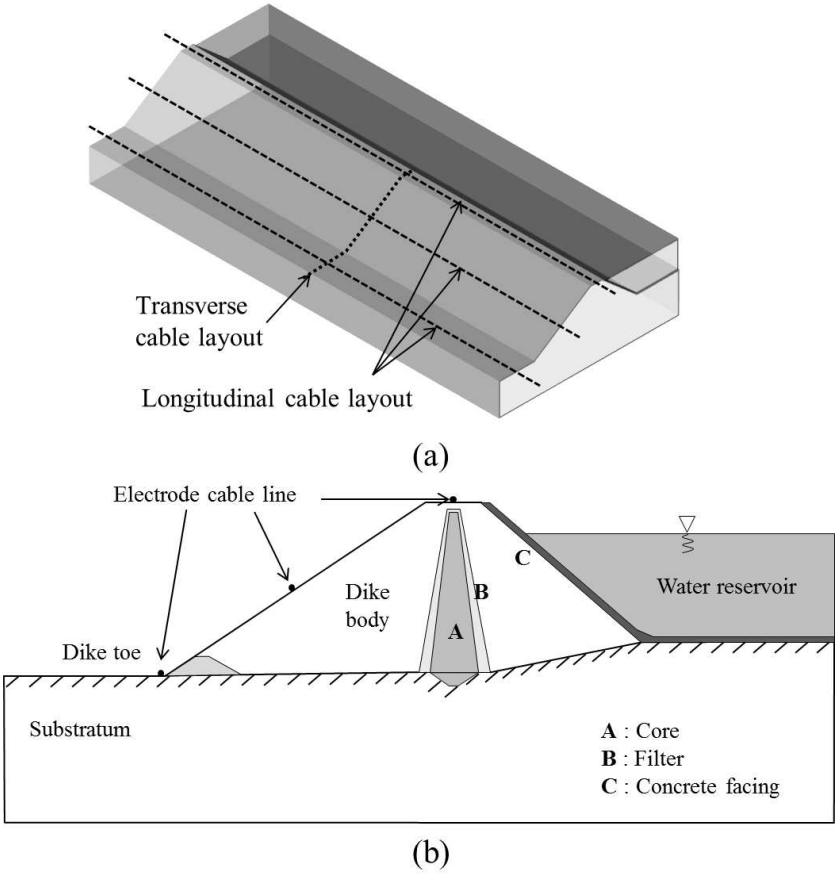

Figure 1: 1(a) Perspective view of a schematic dike with various electrode cable layouts 1(b) schematic section of a dike in load condition presenting some barriers to infiltrations and three longitudinal cable layouts.

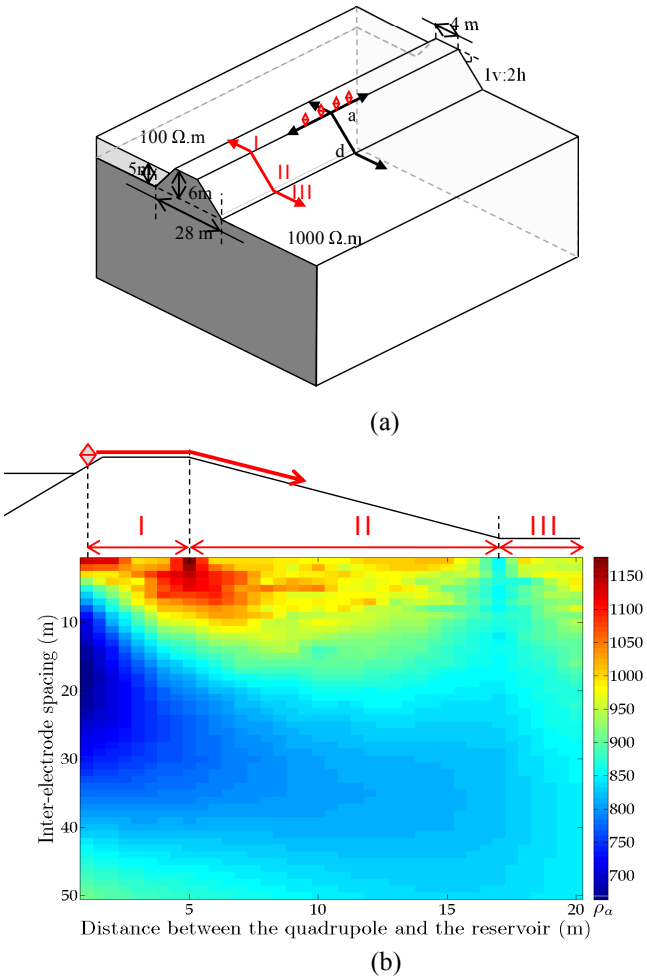

Figure 2: Parametric study of dike geometry and water reservoir effects, 2(a) Simplified dike model showing electrode positions (red diamonds) and 2(b) apparent resistivity plot agaisnt interelectrode spacing and distance between electrode quadrupole and water reservoir. Analytic geometric factors are used for apparent resistivity calculation.

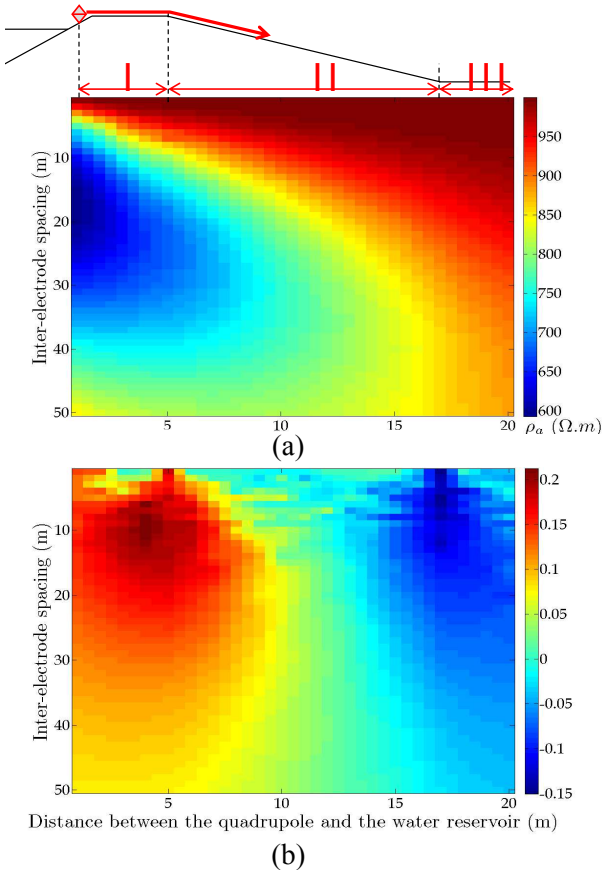

Figure 3: Normalisation effects: 3(a) Apparent resistivities calculated with a generalized geometrical factor obtained by numerical modeling and 3(b) relative variation between the conventional and generalized apparent resistivities.

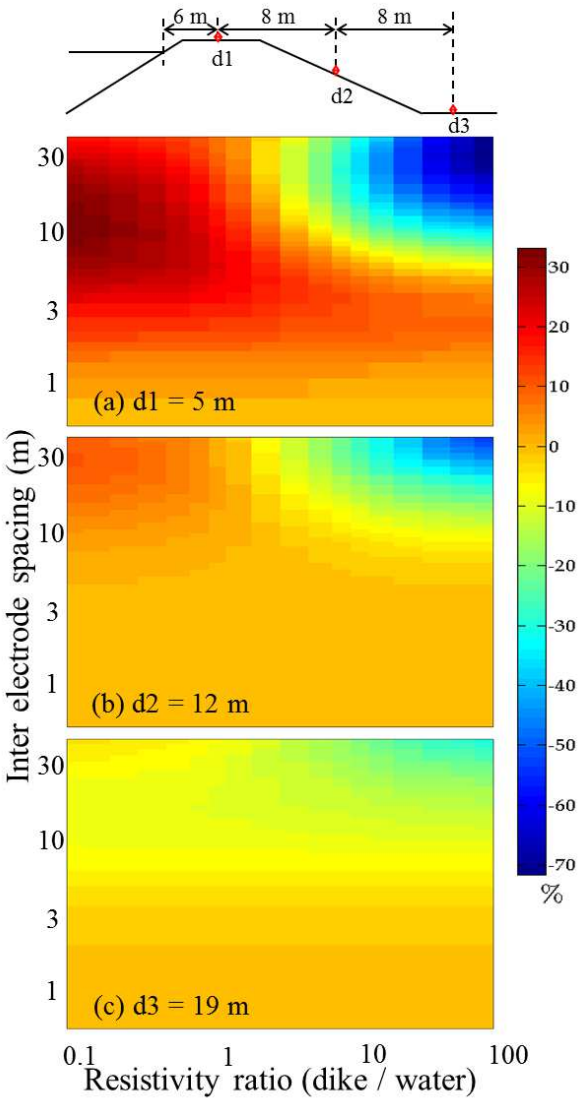

Figure 4: Relative changes in apparent resistivities against inter-electrode spacing and resistivity contrast between water reservoir and dike body (ρ_{water}/ρ_{dike}) for an electrode quadrupole at a distance of (a) 4 m (b) 12 m and (c) 20 m respectively from the water reservoir.

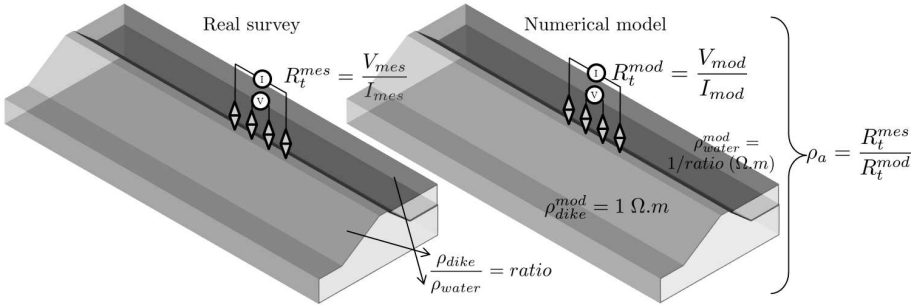

Figure 5: Schematic principle of the Extended Normalisation Technique addionally accounting for the water reservoir effect.

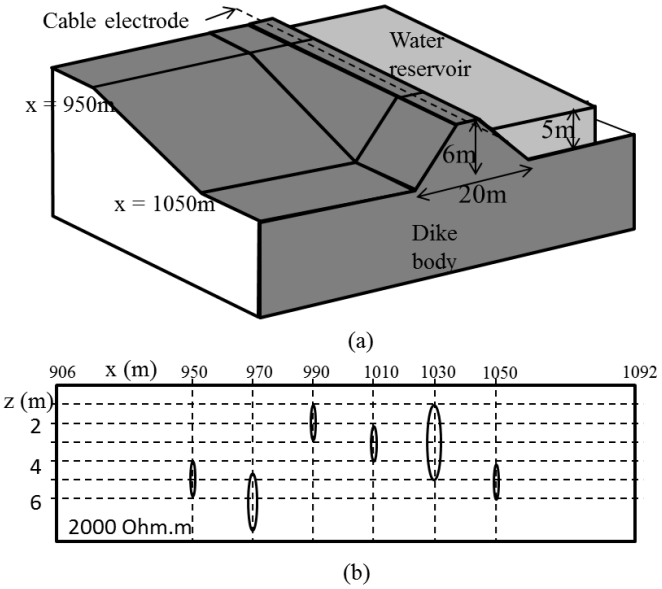

Figure 6: Bloc figure presenting (a) a perspective view of the dike model used for the numerical test exhibiting a varying topography and containing six heterogeneities and (b) a schematic longitudinal section of this model showing the location of the 6 conductive cross-sectional "pipes".

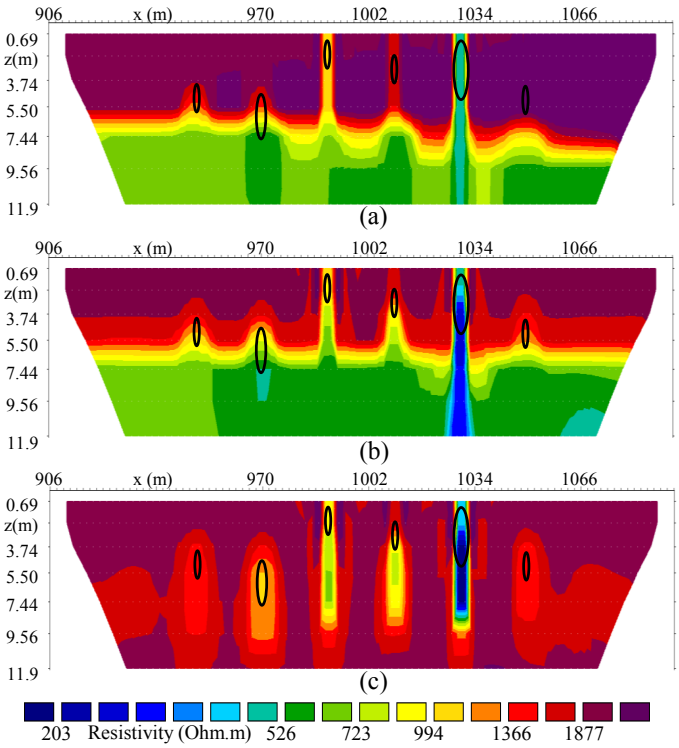

Figure 7: Numerical test 2D-inversion results for (a) simulated ρ_a (without any normalisation) (b) data normalised for the effect of the topography (c) data normalised for the combined effect of the water reservoir and the topography.

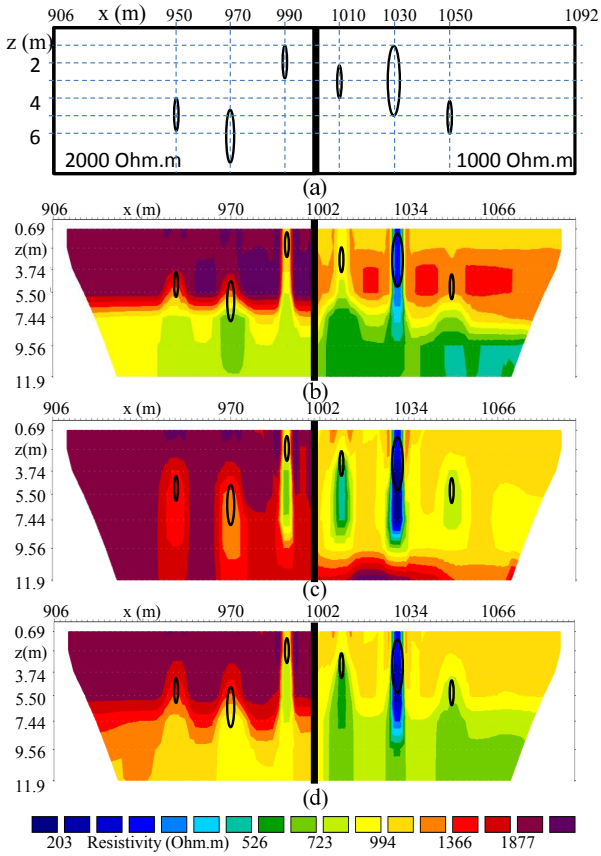

Figure 8: Numerical test demonstrating the limitations due to dike inhomogeneity: (a) a longitudinal section of the dike model composed of two contrasting stretches and the six conductive anomalies and the 2D-inversion results based on (b) raw data (no normalisation applied), (c) with an underestimated and (d) an overestimated resistivity contrast when normalising the data for the combined effect of the water reservoir and the topography.

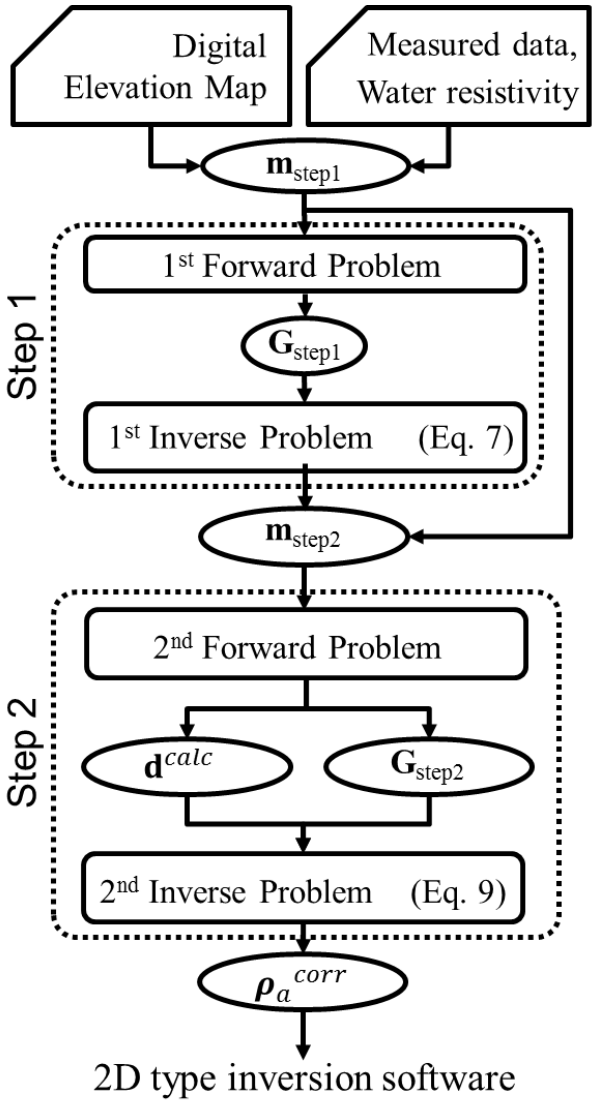

Figure 9: Scheme illustrating the steps of the EEN technique.

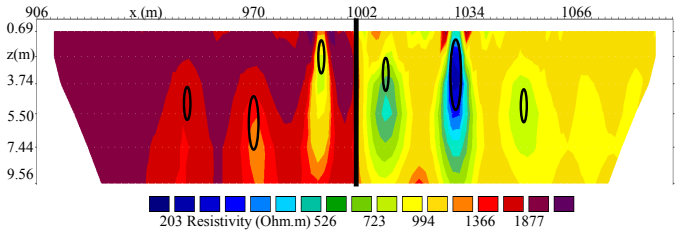

Figure 10: Figure shows the inversion result obtained with apparent resistivity data set normalized with the EEN technique. The true location of the six anomalies and the limit between the stretches are also illustrated.

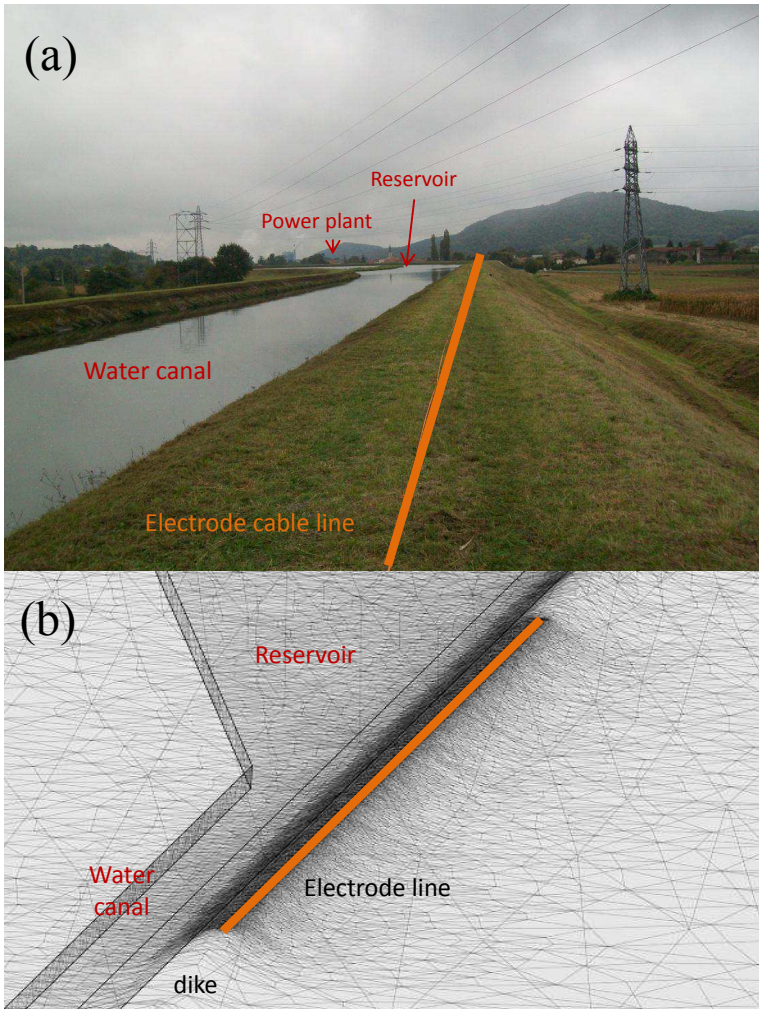

Figure 11: In situ investigation site with 11(a) a view of the survey area and 11(b) the finite element meshing of the numerical model performed by mesh deformation based on the digital elevation map.

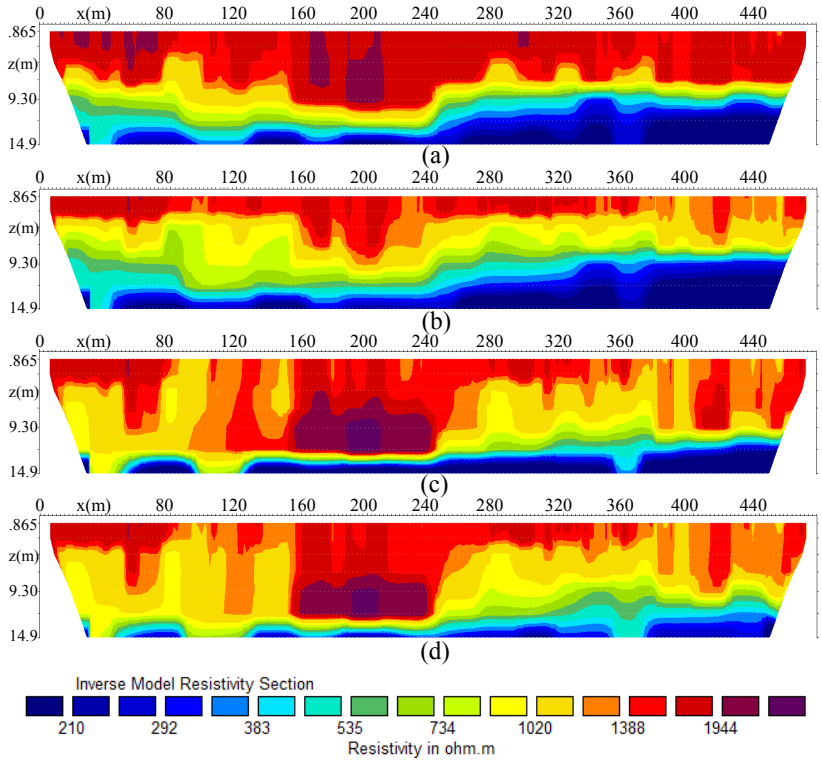

Figure 12: Imaging results obtained with the Res2dinv software for the same set of raw data (a) without any correction (b) normalised for the effect of the topography (c) normalised for the combined effects of the topography and the water reservoir and (d) corrected with the EEN procedure.